PAPER

Cite this: *RSC Adv.*, 2021, **11**, 3110

Synthesis of new M-layer solid-solution 312 MAX phases (Ta$_{1-x}$Ti$_x$)$_3$AlC$_2$ (x = 0.4, 0.62, 0.75, 0.91 or 0.95), and their corresponding MXenes†

Maxwell T. P. Rigby-Bell, [ID] [a] Varun Natu, [b] Maxim Sokol, [bc] Daniel J. Kelly, [a] David G. Hopkinson, [a] Yichao Zou, [a] James R. T. Bird, [ID] [a] Lee J. Evitts, [d] Matt Smith, [a] Christopher P. Race, [a] Philipp Frankel, [a] Sarah J. Haigh [ID] *[a] and Michel W. Barsoum [ID] *[b]

Quaternary MAX phases, (Ta$_{1-x}$Ti$_x$)$_3$AlC$_2$ (x = 0.4, 0.62, 0.75, 0.91 or 0.95), have been synthesised *via* pressureless sintering of TaC, TiC, Ti and Al powders. *Via* chemical etching of the Al layers, (Ta$_{0.38}$Ti$_{0.62}$)$_3$C$_2$T$_z$ – a new MXene, has also been synthesised. All materials contain an M-layer solid solution of Ta and Ti, with a variable Ta concentration, paving the way for the synthesis of a range of alloyed (Ta,Ti)$_3$C$_2$T$_z$ MXenes with tuneable compositions for a wide range of potential applications.

The MAX phases are a class of hexagonal nano-layered carbides and nitrides with general formula M$_{n+1}$AX$_n$, where n = 1, 2, 3, *etc.* and referred to by their stoichiometry – for example M$_2$AX as '211', M$_3$AX$_2$ as '312' and so on. Whilst the 'M' is generally an early transition metal, 'A' an A-group element and 'X' either carbon or nitrogen, all three sites may consist of more than one element in either solid solution or ordered form (such as the M^I, M^{II} ordered 'o-MAX' phases).[1] This vast chemical diversity results in a wealth of material structures and properties, with more than 155 phases known to date – a number that likely represents a small proportion of the material possibilities. The MAX phases have attracted attention due to their interesting mix of ceramic and metallic properties. Like ceramics, some MAX phases are elastically rigid (Young's modulus > 300 GPa),[2] strong at high temperatures,[3] lightweight (<4.5 g cm^{-3}) and creep and oxidation resistant.[4,5] Like metals, MAX phases have shown excellent electrical and thermal conductivity,[6,7] machinability,[8] thermal shock resistance[8] and even damage tolerance.[9] Recently, the interest in MAX phase materials has increased dramatically because they are the feedstock for their two-dimensional derivatives, MXenes.[10] MXenes are typically obtained *via* etching of the MAX phase 'A-layer' and subsequent

chemical delamination of the two-dimensional 'MX-layers'. They have the general formula M$_{n+1}$X$_n$T$_z$, where T$_z$ refers to the MX-layer surface terminations – usually –OH, –O, and/or –F.[11,12] MXenes have shown potential for use in a large range of applications, including photo- and electro-catalysis,[13,14] energy storage and conversion,[15,16] the development of novel hybrid nanocomposites,[17,18] biosensors,[19] water purification,[20] electromagnetic interference shielding,[21] lubrication,[22] and conductive inks.[23,24]

The discovery of new MAX phases and, by extension, new MXenes with different/improved properties can thus be highly valuable. Here we report on the successful synthesis of a range of 312 MAX phase materials, where M is a solid solution of Ta and Ti with variable Ti : Ta ratios, A = Al and X = C. The work builds on previous experimental reports of a 211 MAX phase with similar elemental components – (Ta$_{1-x}$Ti$_x$)$_2$AlC (0 < x < 1),[25] and the pure M-layer 312 MAX phases M$_3$AlC$_2$ (M = Ta or Ti).[26,27] Our experimental realisation of the (Ta$_{1-x}$Ti$_x$)$_3$AlC$_2$ (0 < x < 1) system was motivated by recent theoretical predictions demonstrating the phase stability of TaTi$_2$AlC$_2$ and Ta$_2$TiAlC$_2$ by Dahlqvist and Rosen.[28] We further demonstrate successful exfoliation of (Ta$_{0.38}$Ti$_{0.62}$)$_3$AlC$_2$ to generate a new MXene composition (Ta$_{0.38}$Ti$_{0.62}$)$_3$C$_2$T$_x$.

Synthesis of the (Ta$_{1-x}$Ti$_x$)$_3$AlC$_2$ quaternary, with nominal starting compositions of x = 0.5, 0.66, 0.8, 0.90 and 0.95, was investigated starting from TaC, TiC, Ti and Al powders (Tables S1 and S2, ESI†). Powder mixtures were uniaxially cold-pressed at 250 MPa before being heated to 1600 °C for 8 h in a pressureless flowing Ar tube furnace. Powder X-ray diffraction (XRD) analysis showed each sample contained peaks consistent with

[a] Department of Materials, University of Manchester, Manchester, M1 3BB, UK. E-mail: sarah.haigh@manchester.ac.uk

[b] Department of Materials Science & Engineering, Drexel University, Philadelphia, PA 19104, USA. E-mail: barsoumw@drexel.edu

[c] Department of Materials Science and Engineering, Tel Aviv University, Ramat Aviv 6997801, Israel

[d] Nuclear Futures Institute, Bangor University, Gwynedd, LL57 2DG, UK

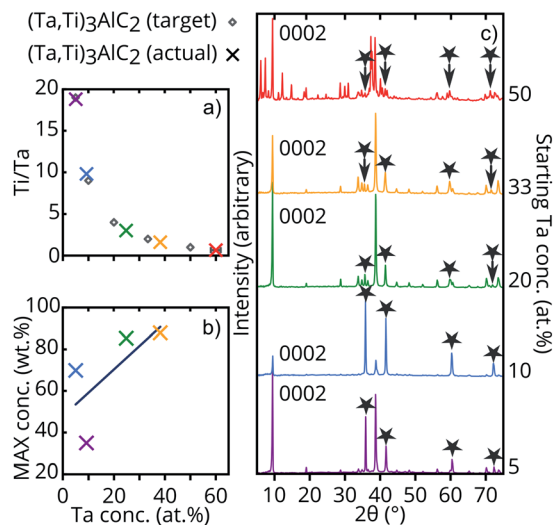**Fig. 1** (a) Ti/Ta fractions for target (diamonds) and actual (crosses) $(Ta,Ti)_3AlC_2$ materials. (b) $(Ta,Ti)_3AlC_2$ MAX phase concentrations in wt%. The x-axis for (a) and (b) is the Ta concentration in at%. (c) XRD diffractograms of as-synthesised materials with variable nominal initial Ta concentrations (right y-axis). The (0002) basal peaks have been identified for the $(Ta_{1-x}Ti_x)_3AlC_2$ phase in each composition, with the positions of $(Ta,Ti)C_x$ ($x \leq 2$) impurity peaks labelled with stars. Actual compositions have been colour coded across all plots.

a hexagonal $P6_3/mmc$ symmetry 312 MAX phase (Fig. 1c), with unit cell volumes ranging from 153.29 ± 0.03 Å^3 (153.29(3) Å^3)‡ to 156.0(1) Å^3 for $(Ta_{0.09}Ti_{0.91})_3AlC_2$ and $(Ta_{0.6}Ti_{0.4})_3AlC_2$ respectively (Table S3, ESI†). A fairly linear increase in cell volume with increasing Ta at% is seen, indicating increasing substitution of the Ti M-site with Ta (atomic radius of 1.45 Å compared to 1.40 Å).[29] This puts the cell volumes in the expected range between the reported value of 151.8(2) Å^3 for Ti_3AlC_2, and the value of 158.73(1) Å^3 reported for Ta_3AlC_2,[27,30] as expected (Fig. S3, ESI†). The highest phase purity of better than 85 wt% was obtained for Rietveld refined compositions of $(Ta_{0.25}-Ti_{0.75})_3Al_{0.77}C_2$ and $(Ta_{0.38}Ti_{0.62})_3Al_{0.81}C_2$ (Fig. 1 and Table S2, ESI†).

The best fitting of the XRD data was achieved with the Al layer arranged in the α-312 stacking configuration for $(Ta_{0.25}-Ti_{0.75})_3Al_{0.77}C_2$, $(Ta_{0.38}Ti_{0.62})_3Al_{0.81}C_2$ and $(Ta_{0.6}Ti_{0.4})_3AlC_2$, with $(Ta_{0.05}Ti_{2.95})_3AlC_2$ and $(Ta_{0.09}Ti_{0.91})_3AlC_2$ arranged in the β-312 configuration (see Table S3, ESI†). For most of the samples, the major impurity peaks were those belonging to cubic $(Ta,Ti)C_x$ ($x \leq 2$) and small quantities of Al_2O_3 and $TiAl_2$ (for discussion, see 'XRD', ESI†). The sample with the highest starting Ta content (50 at%), however, produced a multitude of additional phases, including at least two that have not been identified. As such, structural refinement used a combination of the Rietveld and Pawley methods, that indicated the presence of the expected 312 MAX phase as well as up to five further MAX phases ('XRD' and Fig. S4, ESI†).[31] The lower purity and presence of these extra

‡ Herein this error notation will be used, in which the number in parentheses is the numerical value of the standard uncertainty referred to the corresponding last digit of the quoted result.
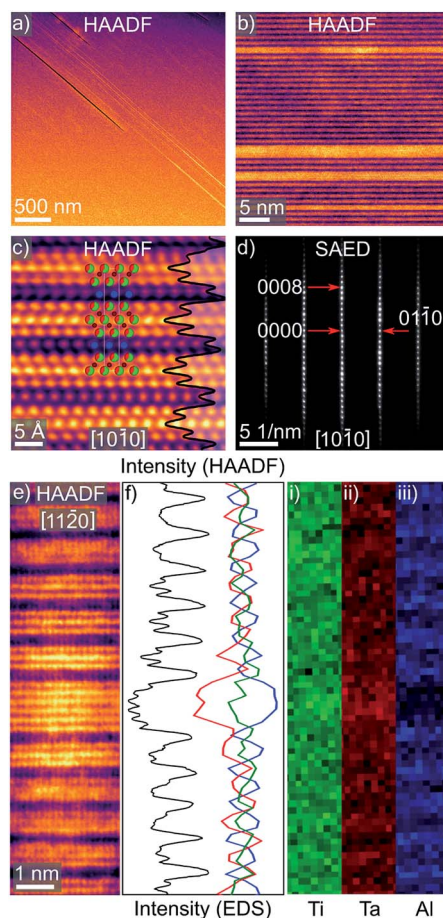

Fig. 2 (a–c) STEM micrographs at varying magnifications of β-$(Ta_{0.38}Ti_{0.62})_3Al_{0.81}C_2$, viewed along the $[10\bar{1}0]$ zone axis. (c) has been Fourier filtered, with the refined structural model overlaid and the unit cell outlined in white. Ti, Ta, Al and C atoms are represented by green, red, blue and brown spheres, respectively. Additionally, an integrated HAADF intensity line profile has been overlaid. (d) SAED micrograph obtained viewing along the same zone axis, with the (0008) and (01$\bar{1}$0) lattice plane reflections identified by red arrows. (e) HAADF STEM micrograph with a stacking fault near the centre, as viewed along the $[11\bar{2}0]$ zone axis. (f) Integrated horizontal line scan profile of (e) (black line), with compositional line profiles obtained from the elemental maps in (i), (ii) and (iii), representing EDS profiles of Ti, Ta and Al in green, red and blue respectively.

phases at the highest Ta concentration suggests a Ta solubility limit in the Ti M-layers.

Energy dispersive X-ray spectroscopy (EDS) implemented within a scanning electron microscope (SEM) was also used for characterisation. EDS provided mean Ti : Ta ratios in the primary phase regions that decreased with increasing Ta concentrations in the starting mixtures (Fig. 1a). In particular, the sample with intended formula $(Ta_{1/3}Ti_{2/3})_3AlC_2$ produced a Ti : Ta ratio of 1.62 : 1 compared with the expected 2 : 1 from the starting mixture (Table S2, ESI†). This is due to the formation of Ti-rich $(Ta,Ti)C_x$ ($x \leq 2$) impurities during synthesis (see 'XRD', ESI†). Both SEM- and scanning transmission electron microscope (STEM) EDS quantitative analysis indicated a sub-stoichiometric Al content in $(Ta_{0.25}Ti_{0.75})_3Al_{0.77}C_2$ and

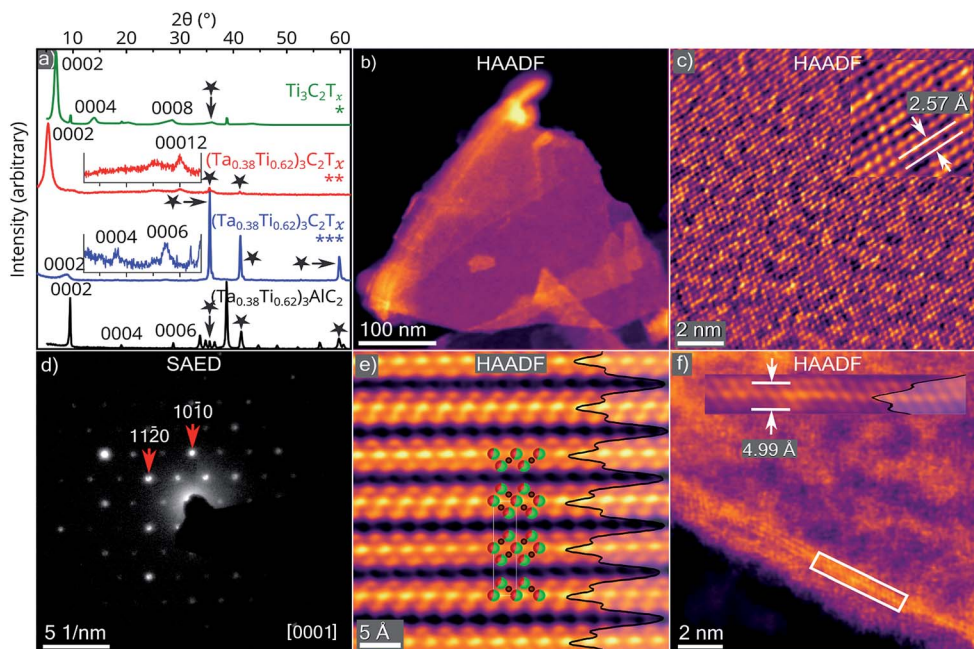**Fig. 3** (a) XRD scans of $Ti_3C_2T_z$ MXene partially intercalated with H_2O (*), delaminated $(Ta_{0.38}Ti_{0.62})_3C_2T_z$ MXene (**), ML $(Ta_{0.38}Ti_{0.62})_3C_2T_z$ MXene (***) and $(Ta_{0.38}Ti_{0.62})_3Al_{0.81}C_2$. A variety of basal plane peaks have been identified, with $(Ta,Ti)C_x$ impurity peaks identified with stars. Additionally, portions of the central two scans have been rescaled to emphasise basal peaks (insets). (b) STEM micrograph of a $(Ta_{0.38}Ti_{0.62})_3C_2T_z$ MXene flake suspended on a holey C-film. (c) Atomic resolution STEM micrograph of the surface of the flake in (b) viewed close to the $[64\bar{1}01]$ zone axis, with a magnified and filtered portion (inset) showing the interatomic spacing. (d) SAED micrograph of a single flake, as viewed along the $[0001]$ zone axis, with the $(10\bar{1}0)$ and $(11\bar{2}0)$ lattice plane reflections labelled. (e) Atomic resolution HAADF STEM micrograph of pristine ML MXene as viewed along the $[10\bar{1}0]$ zone axis, with a proposed structural model overlaid. Ti, Ta and C atoms are represented by green, red and brown spheres, respectively. Additionally, an integrated HAADF intensity line profile has been overlaid in black. (f) STEM micrograph of a $(Ta_{0.38}Ti_{0.62})_3C_2T_z$ flake, with a monolayer edge curled up to align along the $[10\bar{1}0]$ viewing axis. Inset: magnified and filtered view of the white box with an integrated vertical line profile overlaid.

$(Ta_{0.38}Ti_{0.62})_3Al_{0.81}C_2$. Synthesis trials with increased nominal starting Al stoichiometries as high as 1.6 resulted in a decrease in MAX phase purity and increasing quantities of Al_2O_3 and $TiAl_2$. This suggests that the reduced Al occupancy is a thermodynamic effect rather than being due to a deficiency of Al in the starting mixture.

The characteristic 312 MAX phase layered structure of $(Ta_{0.38}Ti_{0.62})_3Al_{0.81}C_2$ can be seen in the high angle annular dark field (HAADF) STEM micrographs in Fig. 2c and e, aligned with the $[10\bar{1}0]$ and $[11\bar{2}0]$ zone axes, respectively. The positions of Al in Fig. 2c are consistent with the β-312 stacking configuration, in contrast to the XRD data, which is likely the result of an α–β transformation during TEM sample preparation, as reported by one of us previously.[9] The HAADF STEM data also reveals that the central metal layers (M^{II}) have visibly higher HAADF intensities than the metal layers that sandwich it (M^I) (see Fig. S1, ESI for diagram†), indicative of a higher atomic number and hence a higher Ta concentration. This is in-line with the XRD data, in which M^I and M^{II} Ta site occupancies converged to 0.340(6) and 0.466(7), respectively (Table S2, ESI†). This preferential elemental enrichment is distinct from the full out-of-plane ordering seen in quaternary 312 o-MAX phases with a 2 : 1 M-element starting ratio.[1] Nonetheless, similar preferential enrichment of the centre M^{II} layer has been observed in 312 M-layer solid solution MAX phases such as $(Cr,V)_3AlC_2$.[1,32] Lattice

parameters obtained from selected area electron diffraction (SAED) patterns, like in Fig. 2d, of $a = 3.01(2)$ Å and $c = 18.59(2)$ Å, are also in good agreement with bulk lattice parameters from XRD ($a = 3.0981(1)$ Å and $c = 18.6140(7)$ Å, see Table S3, ESI†). It should be stressed at this point that the pristine MAX phase layered structure is occasionally interrupted by stacking faults of varying thickness that, at times, penetrate entire crystallites (Fig. 2a, b and e). Structurally, these defects can be thought of as either few-layer ternary carbide impurities, or as MX layers in the MAX phase matrix with an unexpected number of M-layers – such as the 6 shown in Fig. 2e, compared with the expected 3.

High resolution EDS scans, performed over several regions on $(Ta_{0.38}Ti_{0.62})_3Al_{0.81}C_2$ grains, show the expected elemental segregation of Ti, Ta and Al layers, as seen in Fig. 2f(i, ii, and iii), respectively. Quantitative STEM-EDS analysis provided Ti : Ta ratios, excluding stacking faults, from 1.6–1.9 : 1, with a mean value of 1.7(1) : 1, which is close to the 1.62(2) : 1 obtained from SEM-EDS. Note that electron channelling effects and the limited spatial resolution prevent absolute quantification of the relative Ti : Ta concentrations in M^{II} versus M^I sites (see 'Electron microscopy', ESI for methods†).

To demonstrate the potential to produce solid solution Ta/Ti MXenes, we used an in situ HF etching process at 20 °C for 12 h, similar to that performed by Ghidiu et al.[33] (see 'Synthesis', ESI†). Etching of the $(Ta_{0.38}Ti_{0.62})_3Al_{0.81}C_2$ sample produced the

expected $(Ta_{0.38}Ti_{0.62})_3C_2T_z$ MXene (Fig. 3). Characteristic multilayer (ML) flakes were observed following vacuum drying of the MXene suspension (Fig. 3b), with SEM-EDS analysis revealing a 2 : 1 Ti : Ta ratio over micrometre sized areas – including contributions from Ti-rich $(Ta,Ti)C_x$ impurities (similar to the parent MAX phase sample). The etching resulted in a c-lattice parameter increase from 18.6140(7) Å to 19.7(1) Å (Fig. 3a). After sonication, this increased dramatically to 34.9(4) Å, indicating full intercalation of the MX-layers. This suggests a similar formation mechanism to that proposed for producing $Ti_3C_2T_z$ MXene from the parent Ti_3AlC_2 MAX phase, where Al is replaced by terminating species in the etchant such as –OH, –F, or =O, followed by intercalation of the MX-layers by Li^+, allowing for full delamination *via* sonication.[10,15,34] The lower intensity of $(Ta,Ti)C_x$ peaks in the XRD of the delaminated MXene compared to the parent MAX phase (Fig. 3a) suggests an improvement in the purity of the sample (better than the 87.9(2) at% of the parent MAX phase) achieved *via* sonication and centrifugation.

STEM imaging and diffraction was further used to investigate the MXene structure. The pre-delamination $(Ta_{0.38}Ti_{0.62})_3$-C_2T_z ML produced lattice parameters of $a = 3.14(3)$ Å and $c = 11.8(1)$ Å, with a being similar to the parent MAX phase and c reduced following the removal of the Al layer. SAED performed on a fully exfoliated monolayer $(Ta_{0.38}Ti_{0.62})_3C_2T_z$ flake was indexed using a hexagonal basis (Fig. 3d), and produced an a-lattice parameter of 2.97(3) Å, which is in agreement with the value of 2.98(3) Å obtained from fast Fourier transform of the high resolution STEM data (*e.g.* Fig. 3e), and slightly less than the value of 3.0981(1) Å in the parent phase. The monolayer sheet thickness was estimated from HAADF-STEM analysis of the curled-up edge of a single flake as 4.9(5) Å (Fig. 3c) – close to the MX-layer (4.85(2) Å) in the parent phase. Furthermore, the HAADF contrast suggests Ta enrichment in the M^{II} layer relative to the M^I layer, as also observed in the parent MAX phase.

Conclusions

In summary, a new quaternary $(Ta_{1-x}Ti_x)_3AlC_2$ phase system has been synthesised with a variable Ta : Ti ratio ($x = 0.4$, 0.62, 0.75, 0.91 or 0.95) and up to 87.9(2) at% purity. The 'M' sites exist as a solid solution of Ta and Ti, with a higher concentration of Ta in the central M^{II} layers. Experimental results suggest a mean Ta M-layer concentration limit between 38 and 60 at%, beyond which the formation of several alternative MAX phases is favoured, and thus a significant reduction in phase purity. The $(Ta_{0.38}Ti_{0.62})_3Al_{0.81}C_2$ MAX phase was used to synthesise a new solid solution MXene – $(Ta_{0.38}Ti_{0.62})_3C_2T_z$ – *via* chemical etching, with the synthesis pathway likely to be similar to the unalloyed $Ti_3C_2T_x$ MXene. It is proposed that this approach can be used to synthesise a range of alloyed $(Ta,Ti)_3C_2T_x$ MXenes, with compositions that can be optimised for a wide range of potential applications.

Conflicts of interest

There are no conflicts of interest to declare.

Acknowledgements

Notes and references

1 M. Sokol, V. Natu, S. Kota and M. W. Barsoum, *Trends Chem.*, 2019, 1–14.

2 T. Lapauw, A. K. Swarnakar, B. Tunca, K. Lambrinou and J. Vleugels, *Int. J. Refract. Met. Hard Mater.*, 2018, **72**, 51–55.

3 M. W. Barsoum and M. Radovic, *Annu. Rev. Mater. Res.*, 2011, **41**, 195–227.

4 D. J. Tallman, *On the Potential of MAX phases for Nuclear Applications*, Drexel University, 2015.

5 G. M. Song, Y. T. Pei, W. G. Sloof, S. B. Li, J. T. M. De Hosson and S. van der Zwaag, *Scr. Mater.*, 2008, **58**, 13–16.

6 X. H. Wang and Y. C. Zhou, *J. Mater. Sci. Technol.*, 2010, **26**, 385–416.

7 M. W. Barsoum, T. El-Raghy, C. J. Rawn, W. D. Porter, H. Wang, E. A. Payzant and C. R. Hubbard, *J. Phys. Chem. Solids*, 1999, **60**, 429–439.

8 M. W. Barsoum and T. El-Raghy, *J. Am. Ceram. Soc.*, 1996, **79**, 1953–1956.

9 M. W. Barsoum, *MAX Phases: Properties of Machinable Ternary Carbides and Nitrides*, 2013.

10 M. Naguib, M. Kurtoglu, V. Presser, J. Lu, J. Niu, M. Heon, L. Hultman, Y. Gogotsi and M. W. Barsoum, *Adv. Mater.*, 2011, **23**, 4248–4253.

11 M. Naguib, O. Mashtalir, J. Carle, V. Presser, J. Lu, L. Hultman, Y. Gogotsi and M. W. Barsoum, *ACS Nano*, 2012, **6**, 1322–1331.

12 C. Shi, M. Beidaghi, M. Naguib, O. Mashtalir, Y. Gogotsi and S. J. L. Billinge, *Phys. Rev. Lett.*, 2013, **112**, 1–5.

13 J. Ran, G. Gao, F. T. Li, T. Y. Ma, A. Du and S. Z. Qiao, *Nat. Commun.*, 2017, **8**, 13907.

14 H. Lin, X. Wang, L. Yu, Y. Chen and J. Shi, *Nano Lett.*, 2017, **17**, 384–391.

15 B. Anasori, M. R. Lukatskaya and Y. Gogotsi, *Nat. Rev. Mater.*, 2017, **2**, 16098.

16 X. Zhang, Z. Zhang and Z. Zhou, *J. Energy Chem.*, 2018, **27**, 73–85.

17 Z. Ling, C. E. Ren, M. Q. Zhao, J. Yang, J. M. Giammarco, J. Qiu, M. W. Barsoum and Y. Gogotsi, *Proc. Natl. Acad. Sci. U. S. A.*, 2014, **111**, 16676–16681.

18 M. Carey and M. W. Barsoum, *Mater. Today Adv.*, 2021, **9**, 100120.

19 L. Lenka, T. Bertoka, E. Dosekova, A. Holazova, D. Paprckova, A. Vikartovska, V. Sasinkova, J. Filipb, P. Kasak, M. Jerigova, D. Velic, K. A. Mahmoude and J. Tkaca, *J. Phys. Chem. C*, 2017, **235**, 471–479.

20 Q. Peng, J. Guo, Q. Zhang, J. Xiang, B. Liu, A. Zhou, R. Liu and Y. Tian, *J. Am. Chem. Soc.*, 2014, **136**, 4113–4116.

21 F. Shahzad, M. Alhabeb, C. B. Hatter, B. Anasori, S. M. Hong, C. M. Koo and Y. Gogotsi, *Science*, 2016, **353**, 1137–1140.

22 X. Zhang, M. Xue, X. Yang, Z. Wang, G. Luo, Z. Huang, X. Sui and C. Li, *RSC Adv.*, 2015, **5**, 2762–2767.

23 W. Yang, J. Yang, J. J. Byun, F. P. Moissinac, J. Xu, S. J. Haigh, M. Domingos, M. A. Bissett, R. A. W. Dryfe and S. Barg, *Adv. Mater.*, 2019, **31**, 1–8.

24 J. Orangi, F. Hamade, V. A. Davis and M. Beidaghi, *ACS Nano*, 2020, **14**, 640–650.

25 S. Sridharan and H. Nowotny, *Zeitschrift fuer Met. Res. Adv. Tech.*, 1983, **74**, 468–472.

26 N. V. Tzenov and M. W. Barsoum, *J. Am. Ceram. Soc.*, 2000, **83**, 825–832.

27 J. Etzkorn, M. Ade and H. Hillebrecht, *Inorg. Chem.*, 2007, **46**, 1410–1418.

28 M. Dahlqvist and J. Rosen, *Nanoscale*, 2020, **12**, 785–794.

29 J. C. Slater, *J. Chem. Phys.*, 1964, **41**, 3199–3204.

30 G. P. Bei, V. Gauthier-Brunet, C. Tromas and S. Dubois, *J. Am. Ceram. Soc.*, 2012, **95**, 102–107.

31 G. S. Pawley, *J. Appl. Crystallogr.*, 1981, **14**, 357–361.

32 E. N. Caspi, P. Chartier, F. Porcher, F. Damay and T. Cabioc'h, *Mater. Res. Lett.*, 2015, **3**, 100–106.

33 M. Ghidiu, M. R. Lukatskaya, M. Q. Zhao, Y. Gogotsi and M. W. Barsoum, *Nature*, 2015, **516**, 78–81.

34 L. Verger, V. Natu, M. Carey and M. W. Barsoum, *Trends Chem.*, 2019, **1**, 656–669.